AIAA JOURNAL
Vol. 30, No. 7, July 1992

Improved Method for Solving the Viscous Shock Layer Equations

Rachel Gordon*
Texas A&M University, College Station, Texas 77843
and
R. Thomas Davis†
University of Cincinnati, Cincinnati, Ohio 45221

An improved method for solving the viscous shock layer equations for supersonic/hypersonic flows past blunt-nosed bodies is presented. The method is capable of handling slender to thick bodies. The solution is obtained by solving a coupled set of five equations, built of the four basic viscous shock layer equations and an additional equation for the standoff distance. The coupling of the equations prevents the local iterations divergence problems encountered by previous methods of solution far downstream on slender bodies. It also eliminates the need for local iterations, which were required by previous methods of solution, for a first-order scheme in the streamwise direction. A new global iteration procedure is employed to impose the shock boundary conditions. The procedure prevents the global iteration instability encountered by the basic method of solution and improves the convergence rate of the global iteration procedure of later methods devised to overcome this difficulty. The new technique reduces the computation time by 65–95% as compared to previous methods of solution. The method can efficiently be implemented in vector/parallel computers.

Nomenclature

a^* = body nose radius
C_f = skin friction coefficient, $2\tau_w^*/(\rho_\infty^* U_\infty^{*2})$
C_p^* = specific heat at constant pressure
c^* = viscosity law constant, 198.69°R
H = nondimensional total enthalpy, H^*/U^{*2}
h_1, h_2, h_3 = metrics of the coordinate system
k^* = thermal conductivity
M = Mach number
n = nondimensional normal coordinate measured normal to the body surface, n^*/a^*
n_{sh} = nondimensional shock standoff distance, n_{sh}^*/a^*
Pr = Prandtl number, $\mu^* C_p^*/k^*$
p = nondimensional pressure, $p^*/(\rho_\infty^* U_\infty^{*2})$
q = nondimensional heat transfer, $q^*/(\rho_\infty^* U_\infty^{*3})$
Re = Reynolds number, $\rho_\infty^* U_\infty^* a^*/\mu^*(U_\infty^{*2}/C_p^*)$
St = Stanton number, $q_w/(H_o - H_w)$
s = nondimensional longitudinal coordinate measured along the body surface, s^*/a^*
T_∞^*, U_∞^* = freestream temperature and velocity, respectively
t = nondimensional temperature, $t^*/(U_\infty^{*2}/C_p^*)$
u, v = nondimensional velocity components tangent and normal to the body surface, respectively, $u = u^*/U_\infty^*$, $v = v^*/U_\infty^*$
$\bar{u}, \bar{v}$ = nondimensional components of velocity, tangent and normal to the shock interface, respectively
α = shock angle
β = angle between n and negative x direction
γ = ratio of specific heats
Δ = streamwise difference opperator
Δt = time step in the artificial time-like term
δ = iteration difference operator
ε = perturbation parameter, $[\mu^*(U_\infty^{*2}/C_p^*)/\rho_\infty^* U_\infty^* a^*]^{1/2}$
κ = nondimensional surface curvature
μ = nondimensional viscosity coefficient, $\mu^*/\mu^*(U_\infty^{*2}/C_p^*)$
ξ, η = transformed coordinates, $\xi = s$, $\eta = n/n_{sh}$
ρ = nondimensional density, ρ^*/ρ_∞^*
τ = nondimensional shear stress, $\tau^*/(\rho_\infty^* U_\infty^{*2})$
ϕ = body angle; also variable $\phi = \gamma + \omega_p(1 - \gamma)$
$\omega, \omega_2, \omega_3$ = relaxation parameters
$\omega_p, \omega_v, \omega_1$ = weight parameters

Subscripts
i = mesh index measured along the body surface
k = mesh index in direction normal to the body surface
sh = conditions immediately behind the shock
w = wall value
∞ = freestream conditions
0 = stagnation point condition

Superscripts
j = parameter, $j = 0$ for a two-dimensional flow, $j = 1$ for an axisymmetric flow
m, n = local and global iteration number, respectively
$'$ = longitudinal derivative
$*$ = dimensional quantity, also temporary new value

Received May 29, 1990; revision received May 10, 1991; accepted for publication May 10, 1991.

*Visiting Assistant Professor, Department of Aerospace Engineering. Member AIAA.
†(Deceased) Professor, Department of Aerospace Engineering and Engineering Mechanics. Member AIAA.

Introduction

THE calculation of supersonic hypersonic flow past blunt bodies is of prime interest to the designer of re-entry space vehicles. The re-entry flow conditions require the solution to be valid over a wide range of Reynolds numbers, from low Reynolds numbers at high altitude to high Reynolds numbers at low altitude.

At the nose region of blunt bodies, viscous effects influence a significant portion of the shock layer region between the bow shock wave and the body, thereby violating the classical boundary-layer approximation and requiring the use of a more comprehensive set of governing equations. There are several approaches for treating the problem. The first approach is based on coupling the second-order boundary-layer equations solution with the inviscid solution.[1-3] This approach may lead to computational difficulties in the matching procedure on long bodies, at the far downstream region, where strong vorticity interaction occurs.

The second approach is to use the full Navier-Stokes equations.[4,5] This approach has been successful in providing a solution at the stagnation region, but generally has been applied for only 1–2 nose radii downstream. The complexity of this solution restricts its application in the downstream region.

The third approach is to employ the viscous shock layer (VSL) equations. This approach was proposed by Davis and Flügge-Lotz[2] and elaborated into a computational method in Refs. 6–9. It is based on using a combined set of equations obtained from the full Navier-Stokes equations by keeping terms up to second order in the inverse square root of Reynolds number from both a viscous and an inviscid viewpoint. The resulting set of equations is of a boundary-value type; the solution depends on the shock standoff distance distribution and on the downstream pressure and normal component of velocity fields, which are unknown a priori. A global iteration procedure is devised to reflect the boundary-value nature of the equations. This procedure is combined according to the basic method of Ref. 6, with a local iteration procedure devised to solve the governing equations at each streamwise station. If the pressure gradient normal to the body surface is assumed to be established entirely by centrifugal effects, the thin shock layer approximation is obtained.

The main difficulties with the method of Ref. 6 were identified as the shock-shape divergence problem, which becomes severe for thick or slender bodies, and the slow convergence, or sometimes even divergence problem of the local iterations, especially far downstream on slender bodies. In spite of these difficulties, many very useful techniques were developed using this approach for calculating complicated flows.[10,11]

Some improvements to the method were devised in the work of Refs. 12–15. These improvements consisted of reformulation of the manner in which the shock conditions were handled.[12,13] This resolved the shock-shape divergence problem for flows over slender-to-moderate thick bodies. Next, changes were made in the code to couple the normal momentum and the continuity equations,[14] and later also the set of four shock layer equations,[15] to eliminate the local iterations divergence problem occurring far downstream on slender bodies.

In this paper, we present an improved method for solving the VSL equations. It is based on solving a set of five quasi-linearized difference equations derived from the four basic VSL equations (i.e., the longitudinal momentum, normal momentum, energy, and continuity equations) and an additional equation for the standoff distance. The equations are solved simultaneously as a coupled set of equations. The coupling of the equations has the following advantages: it prevents the divergence problems encountered far downstream on slender bodies; it eliminates the need for local iterations at each streamwise station, which were required by previous methods of solution;[6-15] it also makes the method suitable for use on modern parallel/vector computers. A new global iteration procedure is employed to impose the shock boundary conditions. The procedure prevents the shock-shape divergence problem of the basic method of Ref. 6 and improves the convergence rate of the methods of Refs. 12–15 devised to overcome this difficulty. These changes reduce considerably the computation time of the method as compared to previous VSL methods.

Our method is based on writing the p_ξ and v_ξ terms as a combination of forward and backward differences. This enhances the numerical stability of the scheme and assures the mathematical as well as physical consistency of the problem. The use of weighted differences for p_ξ and v_ξ enables the calculation of flows over thick bodies, where the upstream influence becomes very important; previous VSL methods failed to predict these flows.

Recent studies of Rubin,[16] Lin and Rubin,[17] Barnett and Davis,[18] and others have used forward differences or mixed forward-backward differences for calculating the longitudinal pressure gradient term in solving the parabolized or reduced Navier-Stokes equations. In this work, we use mixed differences with the VSL equations. A theoretical stability analysis justifying this approach is presented.

In the following sections, we first present the method. Then we demonstrate the validity and capabilities of the new technique by solving the flow over hyperboloids of various asymptotic cone angles and comparing our results with other methods' results.

Governing Equations

The VSL equations are written in general orthogonal curvilinear coordinates so that arbitrary geometries can be considered. This formulation is obtained by first writing the Navier-Stokes equations in general orthogonal curvilinear coordinates. Then we omit terms of higher than second order in the inverse square root of Reynolds number from both a viscous and an inviscid viewpoint. The resulting equations are the following.

Continuity:

$$(h_2h_3\rho u)_s + (h_1h_3\rho v)_n = 0 \tag{1a}$$

Longitudinal momentum:

$$\rho\left[\frac{u}{h_1}\frac{\partial u}{\partial s} + \frac{v}{h_2}\frac{\partial u}{\partial n} - \frac{v}{h_1h_2}\left(v\frac{\partial h_2}{\partial s} - u\frac{\partial h_1}{\partial n}\right)\right] = -\frac{1}{h_1}\frac{\partial p}{\partial s} + \frac{\varepsilon^2}{h_1^2h_2h_3}\frac{\partial}{\partial n}\left[\frac{\mu h_1^2h_3}{h_2}\left(\frac{\partial u}{\partial n} - \frac{u}{h_1}\frac{\partial h_1}{\partial n}\right)\right] \tag{1b}$$

Normal momentum:

$$\rho\left[\frac{u}{h_1}\frac{\partial v}{\partial s} + \frac{v}{h_2}\frac{\partial v}{\partial n} - \frac{u}{h_1h_2}\left(u\frac{\partial h_1}{\partial n} - v\frac{\partial h_2}{\partial s}\right)\right] = -\frac{1}{h_2}\frac{\partial p}{\partial n} \tag{1c}$$

which with the thin shock layer approximation this becomes

$$\frac{\rho u^2}{h_1}\frac{\partial h_1}{\partial n} = \frac{\partial p}{\partial n} \tag{1d}$$

Energy equation:

$$\rho\left[\frac{u}{h_1}\frac{\partial t}{\partial s} + \frac{v}{h_2}\frac{\partial t}{\partial n}\right] = \frac{u}{h_1}\frac{\partial p}{\partial s} + \frac{v}{h_2}\frac{\partial p}{\partial n} + \varepsilon^2\mu\left[\frac{h_1}{h_2}\frac{\partial(u/h_1)}{\partial n}\right]^2 + \frac{\varepsilon^2}{h_1h_2h_3}\frac{\partial}{\partial n}\left(\frac{h_1h_3}{h_2}\frac{\mu}{Pr}\frac{\partial t}{\partial n}\right) \tag{1e}$$

The equation of state for a perfect gas and Sutherland's law of viscosity are assumed. These are given by

Equation of state:

$$p = \frac{(\gamma - 1)}{\gamma}\rho t \tag{1f}$$

Viscosity law:

$$\mu = \frac{t^{3/2}(1 + c')}{(t + c')} \tag{1g}$$

where

$$c' = \frac{c^*}{M_\infty^2 T_\infty^*(\gamma - 1)} \tag{1h}$$

and c^* is taken to be 198.6°R for air.

Here, h_1, h_2, and h_3 are the metrics of the curvilinear coordinate system and the variables u, v, p, t, ρ, and μ are the nondimensional variables defined by

$$u = \frac{u^*}{U_\infty^*}, \quad v = \frac{v^*}{U_\infty^*}, \quad p = \frac{p^*}{\rho_\infty^* U_\infty^{*2}}, \quad t = \frac{C_p^* t^*}{U_\infty^{*2}}$$

$$\rho = \frac{\rho^*}{\rho_\infty^*}, \quad \mu = \frac{\mu^*}{\mu^\circ(t^* = U_\infty^{*2}/C_p^*)}, \quad \varepsilon = \left(\frac{\mu^\circ}{\rho_\infty^* U_\infty^* a^*}\right)^{1/2}$$

Boundary Conditions

The surface boundary conditions are the no-slip and prescribed wall temperature conditions:

$$u(s, 0) = 0, \quad v(s, 0) = 0, \quad t(s, 0) = t_w \tag{2}$$

The boundary conditions at the shock are the oblique shock relations (see Fig. 1) given by

$$\begin{aligned} u_{sh} &= \tilde{u}_{sh}\sin(\alpha + \beta) + \tilde{v}_{sh}\cos(\alpha + \beta) \\ v_{sh} &= -\tilde{u}_{sh}\cos(\alpha + \beta) + \tilde{v}_{sh}\sin(\alpha + \beta) \end{aligned} \tag{3}$$

where $\tilde{u}_{sh}$ and $\tilde{v}_{sh}$ are the velocity components tangent and normal to the shock interface, respectively, and are given along with the density, pressure, and temperature from the following relations:

$$\tilde{u}_{sh} = \cos\alpha \tag{4a}$$

$$\tilde{v}_{sh} = -\sin\alpha/\rho_{sh} \tag{4b}$$

$$\rho_{sh} = \gamma p_{sh}/(\gamma - 1)T_{sh} \tag{4c}$$

$$p_{sh} = [2/(\gamma + 1)]\sin^2\alpha - (\gamma - 1)/\gamma(\gamma + 1)M_\infty^2 \tag{4d}$$

$$\begin{aligned} t_{sh} = {} & (\tilde{u}_{sh} - \cos\alpha)^2/2 + \{[4\gamma/(\gamma + 1)^2]\sin^2\alpha \\ & + [2/(\gamma - 1) - 4(\gamma - 1)/(\gamma + 1)^2]/M_\infty^2 \\ & - 4/(\gamma + 1)^2 M_\infty^4 \sin^2\alpha\}/2 \end{aligned} \tag{4e}$$

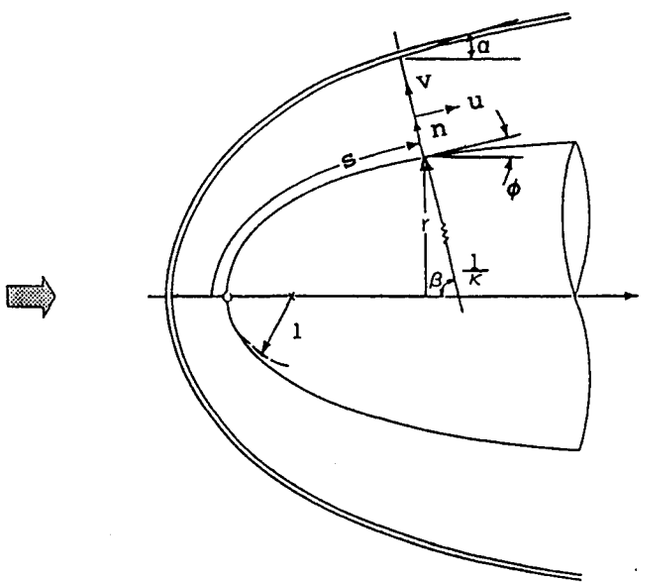

Fig. 1 Body geometry and coordinate system.

Because of the boundary-value nature of the problem, downstream boundary conditions are required for the standoff distance n_{sh} and for the pressure and normal component of velocity in the subsonic region of the downstream boundary. Assuming that the boundary is sufficiently far downstream, these are taken here as n_{sh_ξ} = constant; p_ξ = constant, and v_ξ = constant. Note that the downstream boundary condition on v_ξ is redundant with the thin shock layer approximation.

Transformed Governing Equations

Equations (1a–1e) are now rewritten in the transformed coordinate system (ξ, η) defined by $\xi = s$; $\eta = n/n_{sh}$. This results in the following two second-order and two first-order differential equations:

s-momentum equation:

$$\alpha_o \frac{\partial^2 u}{\partial \eta^2} + \alpha_1 \frac{\partial u}{\partial \eta} + \alpha_2 u + \alpha_3 + \alpha_4 \frac{\partial u}{\partial \xi} = 0 \tag{6a}$$

where

$$\alpha_o = 1 \tag{6b}$$

$$\alpha_1 = \frac{n_{sh}}{\varepsilon^2\mu}\frac{h_2^2}{h_1} n'_{sh}\eta\rho u - \frac{n_{sh}h_2}{\varepsilon^2\mu}\rho v + \frac{\mu_\eta}{\mu} + \frac{1}{h_1}h_{1_\eta} + \frac{h_2}{h_3}(h_3/h_2)_\eta \tag{6c}$$

$$\begin{aligned} \alpha_2 = {} & -\frac{n_{sh}}{\varepsilon^2\mu}\frac{h_2}{h_1}h_{1_\eta}\rho v - \frac{1}{h_1}h_{1_\eta}\frac{\mu_\eta}{\mu} - \frac{1}{h_1}h_{1_{\eta\eta}} \\ & - \frac{h_2}{h_1 h_3}h_{1_\eta}(h_3/h_2)_\eta - \frac{1}{h_1^2}(h_{1_\eta})^2 \end{aligned} \tag{6d}$$

$$\alpha_3 = \frac{n_{sh}^2}{\varepsilon^2\mu}\frac{h_2}{h_1}\rho v^2(h_{2_\xi} - \eta\frac{n'_{sh}}{n_{sh}}h_{2_\eta}) - \frac{n_{sh}^2}{\varepsilon^2\mu}\frac{h_2^2}{h_1}(p_\xi - \eta\frac{\eta'_{sh}}{n_{sh}}p_\eta) \tag{6e}$$

$$\alpha_4 = -\frac{n_{sh}^2}{\varepsilon^2\mu}\frac{h_2^2}{h_1}\rho u \tag{6f}$$

Energy equation:

$$\alpha_o \frac{\partial^2 t}{\partial \eta^2} + \alpha_1 \frac{\partial t}{\partial \eta} + \alpha_2 t + \alpha_3 + \alpha_4 \frac{\partial t}{\partial \xi} = 0 \tag{7a}$$

where

$$\alpha_o = 1 \tag{7b}$$

$$\begin{aligned} \alpha_1 = {} & \frac{n_{sh}}{\varepsilon^2\mu}Pr\frac{h_2^2}{h_1}n'_{sh}\eta\rho u - \frac{n_{sh}}{\varepsilon^2\mu}Prh_2\rho v + \frac{\mu_\eta}{\mu} \\ & + \frac{1}{h_1}h_{1_\eta} + \frac{h_2}{h_3}(h_3/h_2)_\eta \end{aligned} \tag{7c}$$

$$\alpha_2 = 0 \tag{7d}$$

$$\begin{aligned} \alpha_3 = {} & \frac{n_{sh}}{\varepsilon^2\mu}Prh_2^2\left[\frac{n_{sh}u}{h_1}\left(p_\xi - \eta\frac{n'_{sh}}{n_{sh}}p_\eta\right) + \frac{v}{h_2}p_\eta\right] \\ & + Pr\left(u_\eta - \frac{u}{h_1}h_{1_\eta}\right)^2 \end{aligned} \tag{7e}$$

$$\alpha_4 = -\frac{n_{sh}^2}{\varepsilon^2\mu}Pr\frac{h_2^2}{h_1}\rho u \tag{7f}$$

Continuity equation:

$$\frac{\partial}{\partial \xi}(n_{sh}h_2h_3\rho u) + \frac{\partial}{\partial \eta}[h_3\rho(h_1 v - n'_{sh}h_2\eta u)] = 0 \tag{8}$$

n-momentum equation:

$$\alpha_1 \frac{\partial v}{\partial \eta} + \alpha_2 v + \alpha_3 + \alpha_4 \frac{\partial v}{\partial \xi} = 0 \tag{9a}$$

where

$$\alpha_1 = Q\left[-\eta \frac{n'_{sh}}{n_{sh}} \frac{1}{h_1} \rho u + \frac{1}{n_{sh} h_2} \rho v \right] \tag{9b}$$

$$\alpha_2 = Q\left[\frac{1}{h_1 h_2} \left(h_{2_\xi} - \eta \frac{n'_{sh}}{n_{sh}} h_{2_\eta} \right) \rho u \right] \tag{9c}$$

$$\alpha_3 = -\frac{1}{h_1 h_2} \frac{1}{n_{sh}} h_{1_\eta} \rho u^2 + \frac{1}{h_2 n_{sh}} p_\eta \tag{9d}$$

$$\alpha_4 = Q \frac{\rho u}{h_1} \tag{9e}$$

$Q = 0$ for the thin VSL approximation, and $Q = 1$ for the full VSL equations. The remaining equations and boundary conditions are unchanged under this transformation.

This transformation adds a new variable, the standoff distance $n_{sh}(\xi)$. Previous works[6–15] have used local iterations to solve for n_{sh} at each streamwise station. In the present work, we assume n_{sh} to be also a function of η. This yields an additional equation:

$$\frac{\partial n_{sh}}{\partial \eta} = 0 \tag{10}$$

The addition of this equation enables us to get n_{sh} directly by solving a coupled set of equations. Consequently, it eliminates the need for local iterations that were required by previous methods of solution for a first-order scheme in $\Delta\xi$.

Equations (1f), (1g), and (6–10) and the boundary conditions (2–5) constitute a complete set of equations for the unknowns, u, v, t, p, μ, ρ, and n_{sh}.

Method of Solution

The method of solution is as follows. First, an initial guess for the standoff distance $n_{sh}^{(0)}$ is made over the region of interest and its first and second derivatives are calculated. This guess can be arbitrary, but the simplest one is to assume a constant shock thickness. Then, the solution of the equations is obtained by starting at the stagnation point. With an initial guess for the flow profiles at the stagnation point, the quasilinearized equations, which are given in the next section, are solved simultaneously. This results in new flow profiles and a new value for n_{sh} at this point. The coefficients of the quasilinearized equations are then reevaluated and a new solution is obtained. This process is repeated until the solution converges at this point. The method then steps along the body surface. The flow profiles and the value of n_{sh} at the previous station are used as a first guess in evaluating the matrix coefficients at the new station. The equations are then solved and the method steps to the next station. No local iterations are required (except at the stagnation region) for a first-order scheme in $\Delta\xi$.

Once this procedure has marched over the entire computation region, a new standoff distance distribution $n_{sh}^{(n+1)}$ is calculated from

$$n_{sh}^{(n+1)} = \omega n_{sh}^{(n+1),*} + (1 - \omega) n_{sh}^{(n)} \tag{11}$$

where ω is a relaxation parameter and $n_{sh}^{(n+1),*}$ is the recent sweep value of n_{sh}. Note that the method of Ref. 6 actually uses $\omega = 1.0$.

The first and second derivatives of $n_{sh}^{(n+1)}$ are now evaluated and a new sweep solution is obtained, marching from the stagnation point along the body surface downstream. The procedure is repeated until the solution converges.

Linearization of the Governing Equations

The nonlinear equations 6–9 are quasilinearized as follows. The equations are first rewritten in incremental form:

$$f^{(m+1)} = f^{(m)} + \delta F \tag{12}$$

where f stands for any one of the variables u, v, p, t, and n_{sh}, and the superscript m is the mth local iteration value. Then, second-order terms are neglected. This results in a linear set of equations for δu, δv, δp, δt, and δn_{sh}. The following relations are used in the linearization process for any functions f and g:

$$(fg)^{(m+1)} = f^{(m)}\delta g + g^{(m)}\delta f + f^{(m)} g^{(m)} \tag{13a}$$

$$f_\eta^{(m+1)} = f_\eta^{(m)} + (\delta f)_\eta \tag{13b}$$

$$f_{\eta\eta}^{(m+1)} = f_{\eta\eta}^{(m)} + (\delta f)_{\eta\eta} \tag{13c}$$

The functions f and g can be expanded about the previous ξ station value or about the previous global sweep value. Expanding f and g about the previous sweep value yields an error of $O(\Delta\xi)^2$ in Eq. (13a). Thus, local iterations (due to nonlinearity) are not necessary for a first-order scheme in $\Delta\xi$. In this case, with $f_i^{(o)} = f_{i-1}$, we get the following linear equations:

s-momentum equation:

$$a_0 \delta u_{\eta\eta} + (a_1 \delta u_\xi + a_3 \delta p_\xi + a_5 \delta n_{sh_\xi}) + (b_1 \delta u_\eta + b_3 \delta p_\eta) + (c_1 \delta u + c_2 \delta v + c_3 \delta p + c_4 \delta t + c_5 \delta n_{sh}) + d = 0 \tag{14}$$

Energy equation:

$$a_0 \delta t_{\eta\eta} + (a_3 \delta p_\xi + a_4 \delta t_\xi + a_5 \delta n_{sh_\xi}) + (b_1 \delta u_\eta + b_3 \delta p_\eta + b_4 \delta t_\eta) + (c_1 \delta u + c_2 \delta v + c_3 \delta p + c_4 \delta t + c_5 \delta n_{sh}) + d = 0 \tag{15}$$

n-momentum equation:

$$(a_2 \delta v_\xi + a_5 \delta n_{sh_\xi}) + (b_2 \delta v_\eta + b_3 \delta p_\eta) + (c_1 \delta u + c_2 \delta v + c_3 \delta p + c_4 \delta t + c_5 \delta n_{sh}) + d = 0 \tag{16}$$

Continuity equation:

$$(a_1 \delta u_\xi + a_3 \delta p_\xi + a_4 \delta t_\xi + a_5 \delta n_{sh_\xi}) + (b_1 \delta u_\eta + b_2 \delta v_\eta + b_3 \delta p_\eta + b_4 \delta t_\eta) + (c_1 \delta u + c_2 \delta v + c_3 \delta p + c_4 \delta t + c_5 \delta n_{sh}) + d = 0 \tag{17}$$

Equation for n_{sh}:

$$\delta n_{sh} = 0 \tag{18}$$

The coefficients a_1, a_2, ... are given in Ref. 19 and are evaluated independently for each equation.

Difference Equations

Equations (14–18) are solved by finite differences. A two-point backward or mixed forward-backward difference is used for the ξ derivatives. Using the previous sweep values to evaluate the forward ξ derivatives results in a purely implicit scheme, with truncation error of order $O(\Delta\xi)$. Previous studies of Davis[6] have shown that the use of a semi-implicit Crank-Nicolson scheme of order $O(\Delta\xi^2)$ is less stable than the purely implicit scheme, whereas the numerical results of the two schemes do not show much difference for a given step size $\Delta\xi$.

In discretizing the second-order longitudinal momentum and energy equations, three-point differences are used for calculating the first and second η derivatives. The finite difference schemes for the first-order normal momentum, continuity, and

n_{sh} equations are obtained by using averaged quantities centered at midpoint $(i, k + 1/2)$ and employing two-point central differences for calculating the η derivatives at this point.

The linearized equations derived from the longitudinal momentum, energy, normal momentum, continuity, and n_{sh} equations are evaluated at points (i, k), (i, k), $(i, k - 1/2)$, $(i, k + 1/2)$, and $(i, k + 1/2)$, respectively. The resulting difference equations are the following.

s-momentum equation:

$$(a_{11}\delta u_{k-1} + a_{13}\delta p_{k-1}) + (b_{11}\delta u_k + b_{12}\delta v_k + b_{13}\delta p_k + b_{14}\delta t_k + b_{15}\delta n_{sh_k}) + (c_{11}\delta u_{k+1} + c_{13}\delta p_{k+1}) = d_1 \tag{19}$$

Energy equation:

$$(a_{21}\delta u_{k-1} + a_{23}\delta p_{k-1} + a_{24}\delta t_{k-1}) + (b_{21}\delta u_k + b_{22}\delta v_k + b_{23}\delta p_k + b_{24}\delta t_k + b_{25}\delta n_{sh_k}) + (c_{21}\delta u_{k+1} + c_{23}\delta p_{k+1} + c_{24}\delta t_{k+1}) = d_2 \tag{20}$$

n-momentum equation:

$$(b_{31}\delta u_k + b_{32}\delta v_k + b_{33}\delta p_k + b_{34}\delta t_k + b_{35}\delta n_{sh_k}) + (c_{31}\delta u_{k+1} + c_{32}\delta v_{k+1} + c_{33}\delta p_{k+1} + c_{34}\delta t_{k+1} + c_{35}\delta n_{sh_{k+1}}) = d_3 \tag{21}$$

Continuity equation:

$$(a_{41}\delta u_{k-1} + a_{42}\delta v_{k-1} + a_{43}\delta p_{k-1} + a_{44}\delta t_{k-1} + a_{45}\delta n_{sh_{k-1}}) + (b_{41}\delta u_k + b_{42}\delta v_k + b_{43}\delta p_k + b_{44}\delta t_k + b_{45}\delta n_{sh_k}) = d_4 \tag{22}$$

n_{sh} equation:

$$-\delta n_{sh_k} + \delta n_{sh_{k+1}} = 0 \tag{23}$$

where $k = 2, 3, \ldots, K - 1$. The expression for the coefficients can be found in Ref. 19.

The wall and shock boundary conditions are written as the following.

At the wall:

$$\delta u_1 = 0, \quad \delta v_1 = 0, \quad \delta t_1 = 0 \tag{24}$$

At the shock:

$$\begin{aligned}
\delta u_{i,K}^{(n+1)} &= \Delta\xi\left(K_1\frac{d\alpha}{d\xi} + K_2\frac{d\phi}{d\xi}\right) + u_{i-1,K} - u_{i,K}^{(n)} \\
\delta v_{i,K}^{(n+1)} &= \Delta\xi\left(K_5\frac{d\alpha}{d\xi} + K_6\frac{d\phi}{d\xi}\right) + v_{i-1,K} - v_{i,K}^{(n)} \\
\delta p_{i,K}^{(n+1)} &= \Delta\xi K_3\frac{d\alpha}{d\xi} + p_{i-1,K} - p_{i,K}^{(n)} \\
\delta t_{i,K}^{(n+1)} &= \Delta\xi K_4\frac{d\alpha}{d\xi} + t_{i-1,K} - t_{i,K}^{(n)}
\end{aligned} \tag{25}$$

The coefficients $K_1, K_2, \ldots, K_6$ and the expression for $d\alpha/d\xi$ as a function of the first and second derivatives of n_{sh} can be found in Ref. 19.

Equations (19–23) and boundary conditions (24–25) define a linear set of equations of order $5K*5K$, with a 5×5 block tridiagonal coefficient matrix. This equation set is solved by the LU decomposition algorithm.

Convergence of the Global Iteration Procedure

The global iterative procedure of Ref. 6 was found to be unstable and diverged after several iterations. To overcome this difficulty, Werle et al.[12] developed a time-relaxation scheme, where the initial guess of the shock standoff distance is relaxed in an artificial time-like manner, using a two sweep algorithm to approach the steady-state solution. Later studies of Srivastava et al.[13] and of Hosny et al.[15] have used the same or a similar approach to overcome this difficulty.

In this study, we use the under-relaxation technique given by Eq. (11) to overcome this problem. This technique is much simpler than that of Refs. 12, 13, and 15 and it also converges faster, as shown in the Results and Discussion section.

Stability Analysis

To understand the stability problems that occur when a space-marching technique is used, let us examine the influence of the p_ξ and v_ξ terms on the mathematical nature of the VSL equations. For simplicity, we consider a two-dimensional flow with zero curvature. With these assumptions, Eqs. (1a–1e) can be written in a vector form as

$$A\frac{\partial F}{\partial x} + B\frac{\partial F}{\partial y} = C\frac{\partial^2 F}{\partial^2 y} \tag{26}$$

where

$$F = \begin{bmatrix}\rho\\ u\\ v\\ p\end{bmatrix}, \quad A = \begin{bmatrix} u & \rho & 0 & 0\\ 0 & \rho u & 0 & \omega_p\\ 0 & 0 & \omega_v\rho u & 0\\ -a^2u & 0 & 0 & u\phi\end{bmatrix}$$

$$B = \begin{bmatrix} v & 0 & \rho & 0\\ 0 & \rho v & 0 & 0\\ 0 & 0 & \rho v & 1\\ -a^2v & 0 & 0 & v\end{bmatrix}$$

$$C = \frac{\mu}{R_e}\begin{bmatrix} 0 & 0 & 0 & 0\\ 0 & 1 & 0 & 0\\ 0 & 0 & 0 & 0\\ \dfrac{-\gamma p}{\rho^2 p_r} & 0 & 0 & \dfrac{\gamma}{\rho p_r}\end{bmatrix}, \quad \phi = \gamma + \omega_p(1 - \gamma)$$

and ω_p and ω_v are the portion of the p_x and v_x derivatives calculated implicitly by the scheme, respectively.

Consider first the inviscid flow region. In this region, the equations reduce to

$$A\frac{\partial F}{\partial x} + B\frac{\partial F}{\partial y} = 0$$

These equations are hyperbolic provided that the eigenvalues of $|B - \lambda A| = 0$ are real and distinct.[20] The eigenvalue problem reduces to the following equation:

$$(v - \lambda u)\{(v - \lambda u)(v - \lambda\omega_v u)(v - \lambda u\phi) - a^2[\lambda^2\omega_p(v - \lambda\omega_v u) + (v - \lambda u)]\} = 0$$

For $\omega_v = 1$, this equation has two identical roots: $\lambda_1 = \lambda_2 = v/u$. Hence, the equation set is not necessarily hyperbolic. However, if we take $\omega_v = 0$ and

$$\omega_p \le \frac{\gamma M_x^2}{1 + (\gamma - 1)M_x^2}$$

we get real and distinct eigenvalues that yield a hyperbolic set of equations and a stable marching technique.

We next consider the viscous flow region by ignoring the first y derivatives in Eq. (26). The resulting equations are

$$A\frac{\partial F}{\partial x} = C\frac{\partial^2 F}{\partial^2 y}$$

These equations are parabolic in the positive x direction provided the eigenvalues of $|C - \lambda A| = 0$ are real and positive.[20] The eigenvalues must be positive in order for the viscosity to produce damping in the streamwise direction. (Actually in Ref. 20 not all of the eigenvalues have to be strictly positive—see page 436). Solving the eigenvalue problem we get the following: for any ω_v, $u > 0$, and

$$\omega_p \leq \frac{\gamma M_x^2}{1 + (\gamma - 1)M_x^2}$$

(the restriction imposed on ω_p in the inviscid flow region), the eigenvalues are real, nonnegative, and two are strictly positive. Hence, the equation set allows a stable marching technique. Note that under these restrictions on u and ω_p, for $\omega_v = 1$, we get two identical roots $\lambda_1 = \lambda_2 = 0$ and $\lambda_3, \lambda_4 > 0$, whereas for $\omega_v = 0$, we get a reduced 3×3 eigenvalue matrix with $\lambda_1 = 0$ and $\lambda_2, \lambda_3 > 0$. Also, with the thin VSL approximation, the v_x term is omitted, hence, there is no restriction on ω_v.

In the present work, both the v_ξ and p_ξ terms are calculated from the previous global sweep, as explained in the next section. This corresponds to $\omega_p = \omega_v = 0$. Based on the above analysis, a stable marching technique is ensured provided that the v_ξ and p_ξ terms are differenced in an appropriate manner. In the subsonic flow region, in order for the elliptic character of the equations to be properly modeled, these terms must introduce the downstream effect. This is done through the use of mixed forward and backward differences, as described in the next section.

Numerical Solution

To obtain a stable technique, the derivative n_{sh_ξ} is calculated as follows. The value of n_{sh_ξ} in terms that arise from the longitudinal derivatives of the flow variables is taken by its value at the previous global sweep, whereas the value of n_{sh_ξ} in terms that arise from the metrics is quasilinearized around the previous streamwise station value of n_{sh}. The same technique was used in Refs. 6 and 12–15 for calculating n_{sh_ξ}. Furthermore, an artificial time-like term is added to equations (14–17). This term is taken as

$$\frac{|n_{sh_{i-1}}^{(n+1),*} - n_{sh_{i-1}}^{(n)}|}{\Delta t} \frac{\delta n_{sh}}{\Delta \xi} \tag{27}$$

where Δt is an input parameter of the computer program.

To account for the strong downstream of the pressure on the upstream flow region, the longitudinal pressure gradient p_ξ is taken as a weighted combination of forward and backward difference gradient terms,

$$\frac{\partial p}{\partial \xi} = \omega_1 \left(\frac{\partial p}{\partial \xi}\right)_B + (1 - w_1)\left(\frac{\partial p}{\partial \xi}\right)_F \tag{28}$$

where $(\partial p/\partial \xi)_F$ and $(\partial p/\partial \xi)_B$ are forward and backward differenced gradient terms, respectively, and ω_1 is a weight parameter that is determined following Vigneron et al.[21] to be

$$\begin{aligned} \omega_1 &= \frac{\gamma M_\xi^2}{1 + (\gamma - 1)M_\xi^2} \quad \text{for } M_\xi < 1 \\ &= 1 \quad \text{for } M_\xi \geq 1 \end{aligned} \tag{29}$$

where M_ξ is the local Mach number component in the ξ direction.

The use of the forward differences for calculating p_ξ provides a path for upstream propagation of information through subsonic portions of the flowfield. In accordance with the theoretical stability analysis, our numerical studies show that mixed differences are required when solving both the full VSL equations or the thin VSL equations. Although, for some flows the downstream effect is less important when solving the thin VSL equations.

The use of mixed forward-backward differences for the p_ξ term requires the pressure field and a boundary condition on the pressure far downstream. A global relaxation procedure is employed to obtain the pressure field. An initial guess is first made for the entire pressure field; then the field is updated until the solution converges according to

$$p_{i,k}^{(n)} = \omega_2 p_{i,k}^{(n),*} + (1 - \omega_2)p_{i,k}^{(n-1)} \tag{30}$$

where the superscript * refers to the recently calculated value obtained by the nth global sweep, and ω_2 is an under-relaxation parameter. In the present calculations, we used $p_{i,k}^{(0)} = 0$, though this is not crucial to the method. Once the pressure field $p^{(n)}$ has been obtained, the pressure gradient for the $(n + 1)st$ global sweep is calculated following Eq. (28):

$$\left(\frac{\partial p}{\partial \xi}\right)_i = \omega_1 \frac{[p_i^{(n)} - p_{i-1}^{(n)}]}{\Delta \xi} + (1 - \omega_1)\frac{[p_{i+1}^{(n)} - p_i^{(n)}]}{\Delta \xi} \tag{31}$$

In solving the *full* VSL, it is necessary to account for the boundary-value nature of the equations that also appears through the v_ξ term. As seen from the stability analysis, the boundary-value character associated with v_ξ is due to the normal momentum equation (1c). Previous VSL techniques[6,12,13,15] have used a completely forward difference for calculating v_ξ, using the previous global sweep values. In the present study, v_ξ is calculated in a similar way to that used for p_ξ. Mixed forward-backward differences are employed together with a global relaxation iteration procedure. Our numerical studies have shown that using mixed forward-backward differences for v_ξ, instead of forward differences alone, results in a more stable procedure, allowing the use of a larger relaxation parameter ω in Eq. (11).

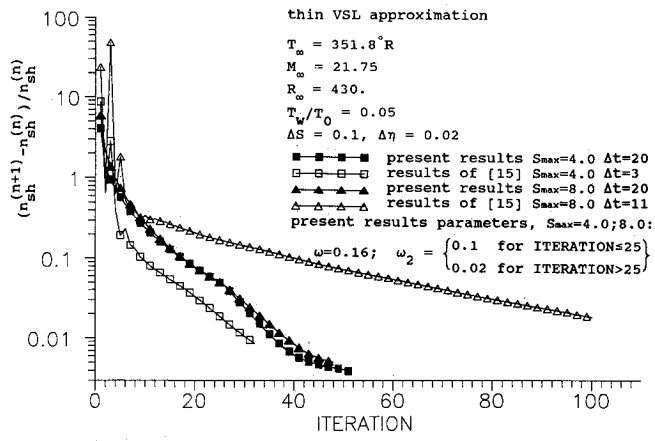

a) 22.5-deg half-angle hyperboloid

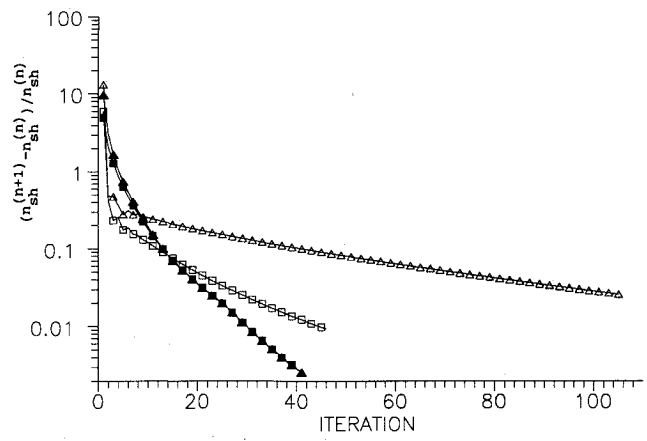

b) 45-deg half-angle hyperboloid

Fig. 2 Standoff distance convergence comparison for flow.

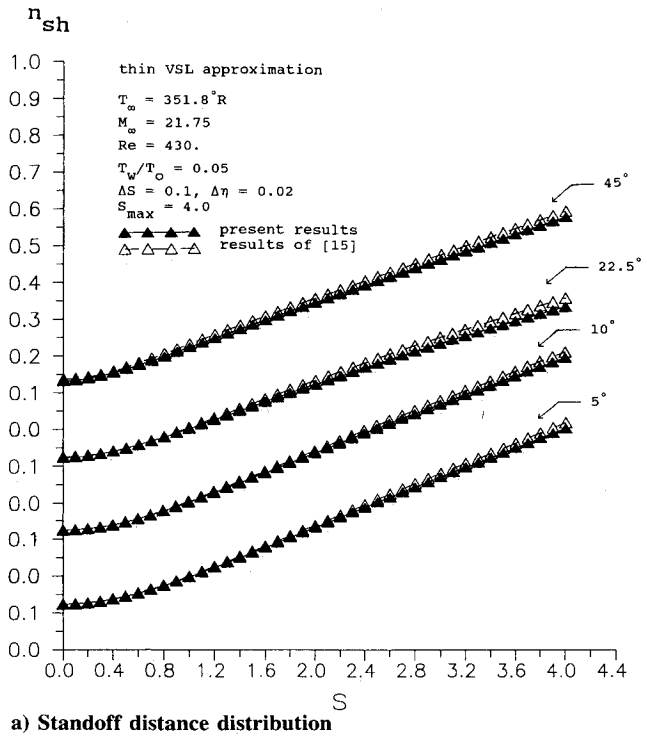

a) Standoff distance distribution

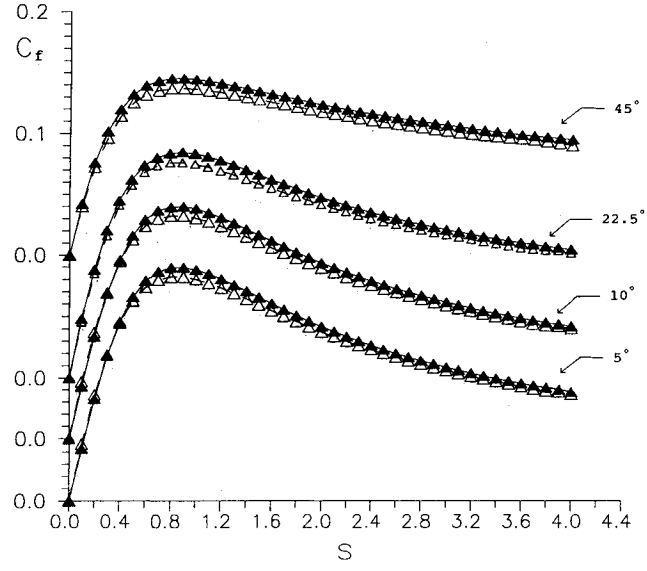

b) Skin friction distribution

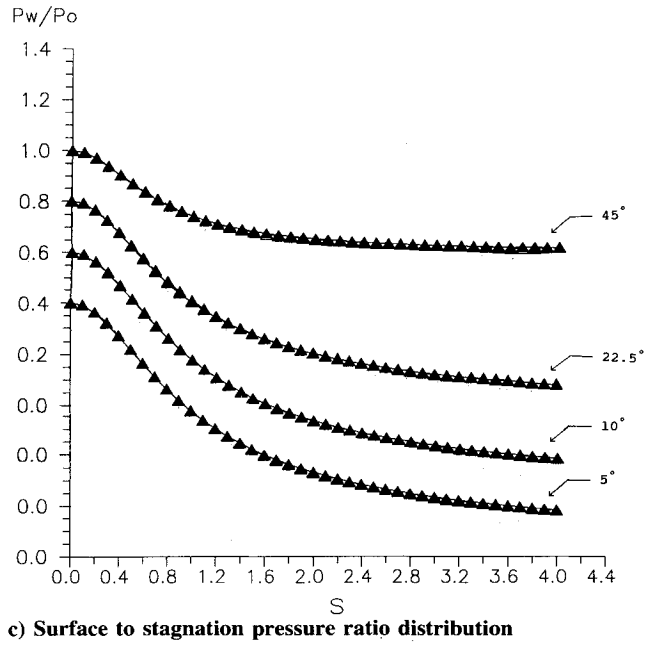

c) Surface to stagnation pressure ratio distribution

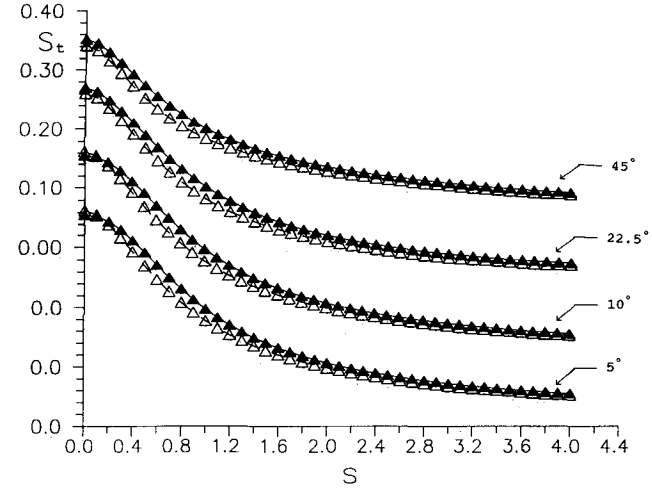

d) Stanton number distribution

Fig. 3 Flow characteristics comparison.

The v_ξ term is calculated as follows. An initial velocity field is first assumed for v, taken here as the first global sweep value. Next, the field is updated using the under-relaxation procedure:

$$v_{i,k}^{(n)} = \omega_3 v_{i,k}^{(n),*} + (1 - \omega_3) v_{i,k}^{(n-1)} \tag{32}$$

where ω_3 is a relaxation parameter. Then, the velocity gradient for the $(n + 1)st$ global sweep is calculated from

$$\left(\frac{\partial v}{\partial \xi}\right)_i = \omega_1 \frac{[v_i^{(n)} - v_{i-1}^{(n)}]}{\Delta\xi} + (1 - \omega_1) \frac{[v_{i+1}^{(n)} - v_i^{(n)}]}{\Delta\xi} \tag{33}$$

The far downstream boundary conditions on the pressure and normal component of velocity are taken here as p_ξ = constant, v_ξ = constant. The constants are unknown a priori and are calculated as part of the global iteration procedure.

Results and Discussion

The numerical algorithm developed in the previous sections is applied here to the solution of the flow over hyperboloids of large to very small asymptotic angles. Results are obtained for the same flow conditions as those considered in Refs. 12 and 15, with a freestream Mach number M_∞ = 21.75, freestream temperature T_∞ = 351.8°R, wall to stagnation temperature T_w/T_o = 0.05, and Reynolds number based on the nose radius Re_∞ = 430. The gas is assumed to be a perfect gas with constant specific heats and a constant Prandtl number Pr = 0.72, and the viscosity is assumed to be given by Sutherland's law.

The initial approximation for the shock is a surface parallel to the body surface at a distance of 0.1072. This is the converged stagnation shock standoff distance value, obtained by Davis' method[6] with the full VSL equations, for a flow over a 22.5-deg half-angle hyperboloid at the same flow conditions. The initial shock shape is not critical to the solution; other smooth shock shapes could be used as well. As to Δt in Eq. (27), our experiments indicate that it should be taken in the range Δt = 1–30. The choice of this parameter does not affect the final converged solution, but it affects the convergence rate of the global iteration procedure. The choice of ω in Eq. (11)

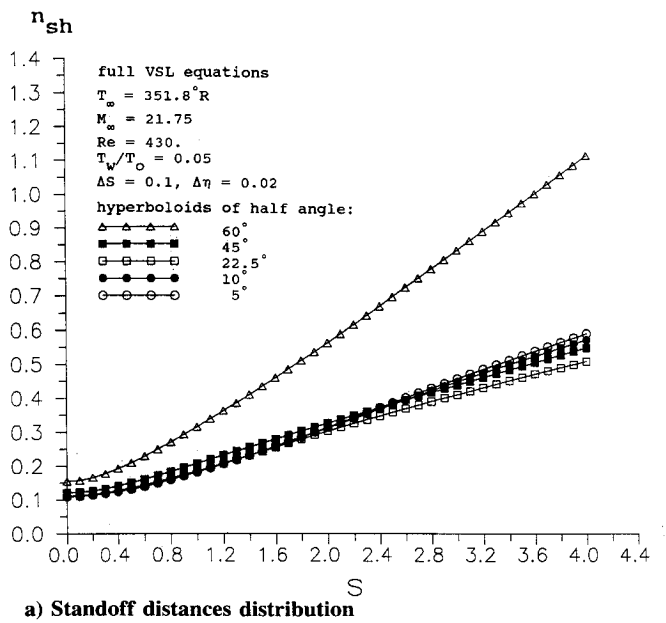

a) Standoff distances distribution

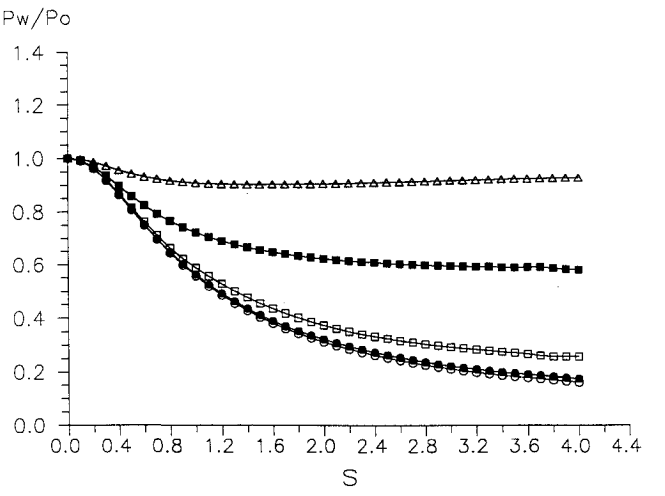

c) Surface to stagnation pressure ratio distribution

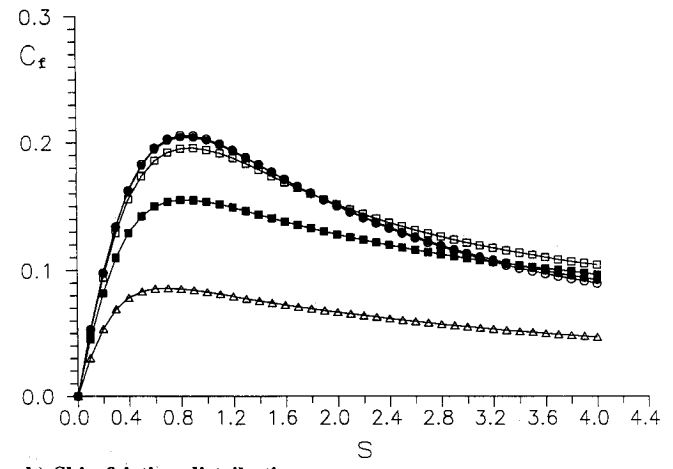

b) Skin friction distribution

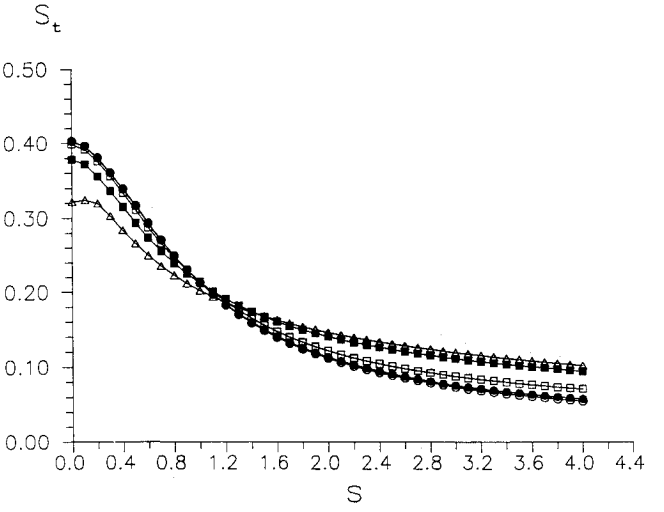

d) Stanton number distribution

Fig. 4 Effect of hyperboloid asymptotic angle on flow characteristics.

affects the convergence rate of the procedure. The use of a large value for ω increases the convergence rate, but may cause oscillations and divergence of the procedure.

Figures 2a and 2b compare the convergence histories of n_{sh} of our method with that of Ref. 15, for S_{max} = 4.0 and 8.0, for flows past 22.5- and 45-deg half-angle hyperboloids, respectively. Near optimal parameters, found by experimentation, were used for both methods; their values are specified in the figures. The parameters of the present method do not change much with the flow case. Note that the definition of convergence of the method of Ref. 15 has been modified here to measure differences between the final sweep and the following star sweep. The original definition of convergence of Ref. 15 (and of Refs. 12 and 13) does not present the actual convergence but a form of cyclic convergence; i.e., it measures convergence by considering the maximum difference between n_{sh} of two successive final sweeps. Differences between n_{sh} of the final sweep and the following star sweep are not considered in Ref. 15 and may still remain quite large at convergence, as actually is the case.

Figures 2a and 2b show that the convergence rate of the present method is almost independent of the length of the calculated region, whereas the convergence rate of Ref. 15 depends strongly on the computed region length, decreasing rapidly with increasing length. For S_{max} = 4.0, the convergence rate of both techniques is similar, whereas for S_{max} = 8.0, the convergence rate of the present method is about four times faster than that of Ref. 15. The convergence rate of the methods of Refs. 12 and 13 is similar to that of Ref. 15.

Our studies show that the relative error for n_{sh} decreases by several orders of magnitude, but eventually, it starts to increase and diverges, with maximum error occurring near the downstream boundary. The stage at which divergence occurs depends on the relaxation parameters ω_1, ω_2, and ω_3. When ω_1 is small enough, divergence depends mainly on ω_2 and ω_3; decreasing these parameters postpones divergence. However, we can prevent divergence and converge to machine zero by holding the pressure and normal component of velocity fields, used for calculating p_ξ and v_ξ, fixed by using $\omega_2 = \omega_3 = 0$. This modification can start at any stage of the process. The divergence is apparently due to our lack of fixed predetermined boundary conditions for p_ξ and v_ξ at the subsonic region of the downstream boundary. By fixing the downstream conditions, we get a mathematically well-posed problem whose solution converges to machine zero. From a practical point of view, the convergence obtained without holding the fields fixed is sufficient and its error is much smaller than the overall numerical error of the method. Moreover, we can hold the pressure and velocity fields fixed when these are converged to within a given convergence criterion and then converge n_{sh} to machine zero.

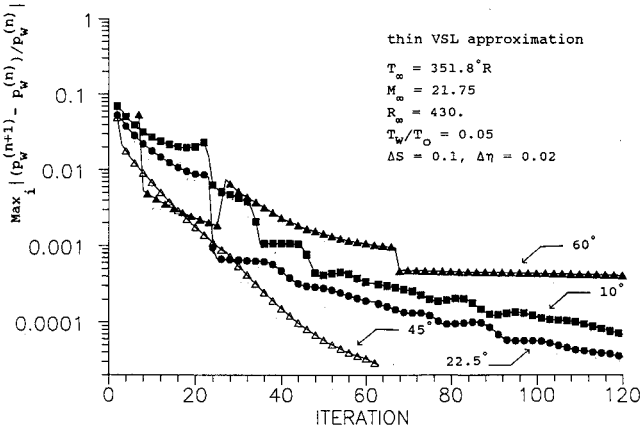

Fig. 5 Convergence histories of maximum wall pressure error for hyperboloids of various asymptotic cone angles.

As a check on the validity of our method of solution, we calculated the flow over 45-, 22.5-, 10-, and 5-deg half-angle hyperboloids and compared the computed results with results of Ref. 15. Figures 3a–d show the calculated results for the standoff distance, skin friction, surface to stagnation pressure ratio, and Stanton number distributions, respectively, as obtained with the thin VSL approximation. These figures show that the present results agree well with results of Ref. 15. The results of Ref. 15 have been compared in Ref. 15 with results of Davis,[6] Werle et al.,[12] and with experimental data and were found to be in good agreement.

To examine the capability of the method of handling slender to thick bodies, we calculated the flow over a wide range of asymptotic cone angle hyperboloids. Figures 4a–d show the calculated results for the standoff distance, skin friction, surface to stagnation pressure ratio, and Stanton number distributions, obtained with the full VSL equations for the 10-, 22.5-, 45-, and 60-deg half-angle hyperboloids. Our studies show that the method of Ref. 15 diverges for the 60-deg half-angle hyperboloid. This is apparently due to inappropriate modeling of the strong downstream effect for this wide body flow case.

Figure 5 presents the convergence histories of the wall pressure ratio for the 22.5-, 45-, and 60-deg half-angle hyperboloids, with the thin VSL approximation. This figure shows that the convergence rate of the 22.5- and 45-deg flow cases is much faster than that of the 60-deg flow case. This is due to the strong downstream effect on the upstream flow region, which becomes very important for the 60-deg flow case. For this case, the calculated flow remains subsonic throughout the flowfield.

The present method reduces the computation time significantly as compared to previous methods of solution of Refs. 12, 13, and 15. This is due to the elimination of the need for local itertions at each streamwise station and the faster global iteration procedure, in cases where the calculations proceed far downstream. The method can be efficiently implemented on vector/parallel machines since the coefficients of the quasilinearized equation set can be evaluated independently.

To compare the CPU time of the present method with that of Ref. 15, we ran the two codes on an IBM 3090 vector computer, though no changes have been made in these codes to utilize the vector features of this machine. The CPU time per iteration of both codes were evaluated by running, for a few iterations, a test case involving 51 nodes in the η direction. Based on this test case, the present code written for the specific metrics used in Ref. 15 requires 0.00925 s per 1 local iteration as compared to 0.00737 s required by the method of Ref. 15. Now, for getting a stable procedure, the method of Ref. 15 requires about 4 local iterations per streamwise station. Hence, the present technique requires about 32% of the CPU time of Ref. 15 per streamwise station. When we account for the total number of global iterations required for convergence, we get a reduction to about 35–10% of the total CPU time or even more, depending on the length of the calculated flow region. Further studies for flows over slender sphere/cone shapes, where local iterations with under-relaxation are required for $s \geq 1.1$, show an even better CPU improvement due to the large under-relaxation parameter that can be used with the present method.

Conclusions

A new method for solving the VSL equations for supersonic/hypersonic flows over axisymmetric blunt bodies or two-dimensional blunt wedges has been presented. The method is capable of handling thick-to-slender body configurations. The results obtained by the method agree well with available results of previous methods. The main advantages of the method are the significant reduction of the computation time as compared to previous methods of solution and its simplicity. The reduction of the computation time is achieved by eliminating the need for local iterations at each streamwise station and the employment of an efficient global iteration procedure. The VSL equations are formulated in general orthogonal curvilinear coordinates so that general body shapes can be handled.

Mixed forward-backward differences are used for the p_ξ and v_ξ terms that are calculated by a global iteration procedure. The use of mixed differences assures the mathematical as well as physical consistency of the problem.

The method can be implemented efficiently on vector/parallel computers since it enables the effective utilization of the special processing features of these machines. The method can be extended to the solution of supersonic/hypersonic flows past blunt-nosed bodies at angles of attack, which are of prime interest at the present.

Acknowledgment

This research was supported by NASA Langley Research Center Grant NAG-1-548 during 1985 and 1987, and continued while the first author was a Koret Fellow at Technion—Israel Institute of Technology.

References

[1]Van Dyke, M., "A Review and Extension of Second Order Hypersonic Boundary-Layer Theory," *Rarefied Gas Dynamics, Fluid Symposium Supplement 2*, edited by J. A. Lauermann, Vol. II, Academic, New York, 1963.

[2]Davis, R. T., and Flügge-Lotz, I., "Second-Order Boundary-Layer Effects in Hypersonic Flow Past Axisymmetric Blunt Bodies," *Journal of Fluid Mechanics*, Vol. 20, Pt. 4, 1964, pp. 593–623.

[3]Marchand, E. O., Lewis, C. H., and Davis, R. T., "Second Order Boundary-Layer Effects on a Slender Blunt Cone at Hypersonic Conditions," AIAA Paper 68-54, Jan. 1968.

[4]Jain, A. C., and Adimurthy, V., "Hypersonic Merged Stagnation Shock Layers, Part II, Cold Wall Case," *AIAA Journal*, Vol. 12, No. 3, 1974, pp. 384–354.

[5]Gupta, R. N., and Simmonds, A. L., "Hypersonic Low-Density Solutions of the Navier-Stokes Equations with Chemical Nonequilibrium and Multicomponent Surface Slip," AIAA Paper 86-1349, June 1986.

[6]Davis, R. T., "Numerical Solution of the Hypersonic Viscous Shock-Layer Equations," *AIAA Journal*, Vol. 8, No. 5, 1970, pp. 843–851.

[7]Whitehead, R. E., and Davis, R. T., "Surface Conditions in Slip Flow With Mass Transfer," Virginia Polytechnic Inst. and State Univ., College of Engineering, Rept. VPI-E-69-11, Blacksburg, VA, 1970.

[8]Whitehead, R. E., and Davis, R. T., "Numerical Solutions to the Viscous Shock-Layer Blunt Body Problem With Inert Gas Injection," Sandia National Lab. Rept., Aero-Thermodynamics SC-CR-70-6162, Albuquerque, NM, Jan. 1971.

[9]Davis, R. T., "Hypersonic Flow of a Chemically Reacting Binary Mixture Past a Blunt Body," AIAA Paper 70-805, June 1970.

[10]Moss, J. N., "Solutions for Reacting and Nonreacting Viscous Shock-Layers with Multicomponent Diffusion and Mass Injection," Ph.D. Dissertation, Virginia Polytechnic Inst. and State Univ., Blacksburg, VA, Oct. 1971.

[11]Anderson, E. C., Moss, J. N., and Sutton, K., "Turbulent Viscous Shock-Layer Solutions with Strong Vorticity Interaction," AIAA Paper 76-120, Jan. 1976.

[12]Werle, M. J., Srivastava, B. N., and Davis, R. T., "Numerical Solutions to the Full Viscous Shock-Layer Equations Using an ADI

Technique," Dept. of Aerospace Engineering, Univ. of Cincinnati, Rept. AFL 74-7-13, Cincinnati, OH, Aug. 1974.

[13]Srivastava, B. N., Werle, M. J., and Davis, R. T., "Viscous Shock-Layer Solutions for Hypersonic Sphere Cones," *AIAA Journal*, Vol. 16, No. 2, 1978, pp. 137–144.

[14]Waskiewicz, J. D., Murray, A. L., and Lewis, C. H., "Hypersonic Viscous Shock Layer Flow over a Highly Cooled Sphere," *AIAA Journal*, Vol. 16, No. 2, 1978, pp. 189–192.

[15]Hosny, W. H., Davis, R. T., and Werle, M. J., "Improvements to the Solution of the Viscous Shock-Layer Equations," Arnold Engineering Development Center, Rept. AEDC-TR-79-25, Aug. 79.

[16]Rubin, S. G., "A Review of Marching Procedures for Parabolized Navier-Stokes Equations," *Numerical and Physical Aspects of Aerodynamic Flows*, edited by T. Cebeci, Springer-Verlag, New York, 1982, pp. 171–185.

[17]Lin, A., and Rubin, S. G., "Three-Dimensional Supersonic Viscous Flow over a Cone at Incidence," *AIAA Journal*, Vol. 20, No. 11, 1982, pp. 1500–1507.

[18]Barnett, M., and Davis, R. T., "A Procedure for the Calculation of Supersonic Flow with Strong Viscous-Inviscid Interaction," AIAA Paper 85-0166, Jan. 1985.

[19]Gordon, R., and Davis, R. T., "An Improved Method for Solving the Viscous Shock Layer Equations," Dept. of Aerospace Engineering, Univ. of Cincinnati, Cincinnati, OH, 1986.

[20]Anderson, A. D., Tannehill, C. J., and Pletcher, H. R., *Computational Fluid Mechanics and Heat Transfer*, Hemisphere, New York, 1984.

[21]Vigneron, Y. C., Rakich, J. V., and Tannehill, J. C., "Calculation of Supersonic Flow over Delta Wings with Sharp Subsonic Leading Edges," NASA TM-78500, June 1978.